

EFFECT OF PRIOR MACHINING DEFORMATION ON THE DEVELOPMENT OF TENSILE RESIDUAL STRESSES IN WELD FABRICATED NUCLEAR COMPONENTS

P. S. Prev y, P. W. Mason, D. J. Hornbach, and J. P. Molkenthin

ABSTRACT

Austenitic alloy weldments in nuclear systems may be subject to stress corrosion cracking (SCC) failure if the sum of residual and applied stresses exceeds a critical threshold. Residual stresses developed by prior machining and welding may either accelerate or retard SCC, depending upon their magnitude and sign. A combined x-ray diffraction and mechanical procedure was used to determine the axial and hoop residual stress and yield strength distributions into the inside diameter surface of a simulated Alloy 600 penetration J-welded into a reactor pressure vessel. The degree of cold working and the resulting yield strength increase caused by prior machining and weld shrinkage was calculated from the line broadening distributions.

Tensile residual stresses on the order of +700 MPa were observed in both the axial and hoop directions at the inside diameter surface in a narrow region adjacent to the weld heat affected zone (HAZ). Stresses exceeding the bulk yield strength were found to develop due to the combined effects of cold working of the surface layers during initial machining, and subsequent weld shrinkage. The residual stress and cold work distributions produced by prior machining were found to strongly influence the final residual stress state developed after welding.

KEYWORDS: residual stress, stress corrosion cracking, machining, welding, Alloy 600

INTRODUCTION

PRIMARY WATER STRESS CORROSION cracking of austenitic alloy weldments, such as 304 stainless steel and Alloy 600, has been observed for decades, and continues to be a primary maintenance concern with both pressurized water and boiling water reactors. Intergranular SCC was observed in several partial J-weld penetrations of both heater sleeve and pressurizer nozzles in nuclear pressure vessels⁽¹⁾. Initial investigations of Alloy 600 sleeves and nozzles prior to welding indicated that the residual stresses produced by machining alone were well below the +276 MPa⁽²⁾ required to initiate stress corrosion cracking.

A series of J-weld mockup specimens consisting of Alloy 600 tubular sleeves welded into a steel block were prepared to simulate the combined effects of machining and welding which occur during fabrication of pressure vessel penetrations. A procedure employing mechanical strain gaging and x-ray diffraction techniques was used to allow exposure of the inside diameter surface and the subsequent measurement of both the macroscopic residual stress and the degree of cold working of the surface. Preliminary results obtained with relatively coarse depth resolution showed a pronounced change in the magnitude of residual stress and cold work with increasing depth into the surface of the sample^(3,4). The purpose of this study was to characterize the residual stress and cold work distributions with higher depth

P.S. Prevey, P.W. Mason, and D.J. Hornbach, Lambda Research, Cincinnati, OH, USA
J.P. Molkenthin, ABB-Combustion Engineering, Windsor, CT, USA

and spatial resolution than was previously achieved, concentrating in the layers deformed by machining prior to welding.

SPECIMEN FABRICATION

Several J-weld heater sleeve mockups were prepared by ABB-Combustion Engineering to simulate as accurately as possible the actual fabrication procedures used in the pressure vessel penetrations which had experienced stress corrosion cracking in service. Mockup specimen #9, which was prepared with a 50 deg. penetration angle, was used in this investigation. The Alloy 600 heater sleeve was taken from decontaminated material removed from a reactor system which had experienced SCC failure. Alloy compositions are given in Table I. The sleeve was fabricated from cold drawn tubing. Portions of the inside surface of the sleeve had been reamed during the original pressure vessel fabrication. The use of portions of decontaminated sleeves which had actually exhibited weld related SCC failure in the field assured that the residual stress and cold work distributions produced by reaming of the sleeves used in the mockups would be identical to that which may have contributed to the field failures.

Element	Alloy 82	Alloy 600
Nickel	72.0	76.0
Chromium	20.0	15.5
Iron	1.0	8.0
Manganese	3.0	0.5
Carbon	0.02	0.08
Sulfur	0.007	0.008
Silicon	0.20	0.25
Copper	0.04	0.25
Titanium	0.55	...
Niobium	2.5	...

Table I - Nominal compositions of Alloy 82 and Alloy 600^(5,6)

A massive carbon steel block nominally 152 mm square at the base was machined from archival SA-533B reactor vessel steel with a 50 deg. penetration

angle as shown in Fig. 1. The surface was overlaid with Alloy 82 weld metal to a nominal depth of 10 mm. The penetration clearance hole was drilled down the axis of the block, and J-weld preparations were machined into the Alloy 82 overlay. The Alloy 600 sleeve was then inserted into the block and welded in place with Alloy 82 filler metal using the same welding parameters and bead deposition sequence prescribed for the original sleeves which had experienced SCC.

EXPERIMENTAL TECHNIQUE

In order to expose the inside diameter surface of the Alloy 600 sleeve for measurement by x-ray diffraction (XRD), it was necessary to section the weld mockups axially along a plane perpendicular to the plane of Fig. 1. The "high" and "low" side weld regions (right and left sides in Fig. 1), where the majority of SCC cracks had occurred in field failures, were then available for measurement. The residual stress relaxation which occurred during sectioning was monitored by installing a series of six biaxial strain gage rosettes on the inside diameter surface, spanning the nominally 64 mm XRD measurement region.

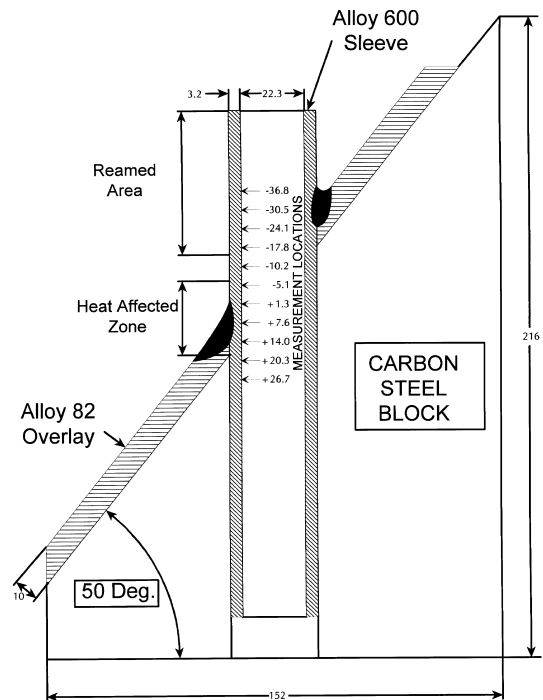


Fig. 1 - Alloy 600 50-deg. heater sleeve penetration J-weld mockup specimen geometry

The residual strain relaxations were interpolated along

the inside surface between the center points of the strain gage grids to provide a continuous distribution of strain relaxation from which the residual stress relaxations at each XRD measurement location were calculated, assuming that the principal stress relaxation directions were in the hoop and axial directions for the simple cylindrical geometry. Only the low (left) side of the J-weld mockup was used for the high resolution study described here. The high side had been used for one of the previous studies.⁽³⁾

The XRD measurement locations shown in Fig. 1 are indicated by the axial displacement from the intersection of the plane defining the top surface of the Alloy 82 overlay and the inside diameter surface of the Alloy 600 sleeve on the low side. These coordinates are used for the presentation of all data obtained on the inside diameter surface in order to maintain reference to the location of the weld.

X-ray diffraction residual stress measurements were made employing a $\sin^2\psi$ technique and the diffraction of manganese or copper $K\alpha$ radiation from the (311) or (420) planes of the austenitic alloy after verification of the linear dependence of the lattice spacing upon $\sin^2\psi$ produced by plane stress at a free surface.⁽⁵⁻⁸⁾ The copper $K\beta$ and iron and chromium $K\alpha$ fluorescent background radiation was suppressed using a high energy resolution solid state Si(Li) detector and single-channel analyzer. The x-ray elastic constants required to calculate the macroscopic residual stress from the strain measured in the (311) and (420) directions were determined empirically⁽⁹⁾ in accordance with ASTM E-1426. Systematic errors due to diffractometer and sample misalignment were monitored in accordance with ASTM E-915. The position and width of the $K\alpha_1$ diffraction peak was separated from the combined $K\alpha$ doublet using Pearson VII function peak profile deconvolution.⁽¹⁰⁾

Previous studies of the nickel-base super alloys Inconel 718 and Rene 95, and the stress-corrosion-resistant Alloys 690 and 600 had shown that an empirical relationship could be established between the $K\alpha_1$ peak width and the degree to which the material was cold worked.⁽¹¹⁾ If the measure of cold work is taken to be the true plastic strain, then the total line broadening is found to be independent of the mode of deformation, whether tensile or compressive, and to be accumulative for complex deformation histories.⁽¹¹⁾

After sectioning, the strain gages were removed chemically from the inside diameter surface, and XRD residual stress measurements were made in both the hoop and axial directions at the measurement locations shown in Fig. 1. Layers of material were then electropolished from the inside surface, and the process repeated to a total depth of nominally 0.25 mm into the inside surface of the sleeve. The diffraction peak width and residual stress distributions were measured simultaneously as functions of depth.

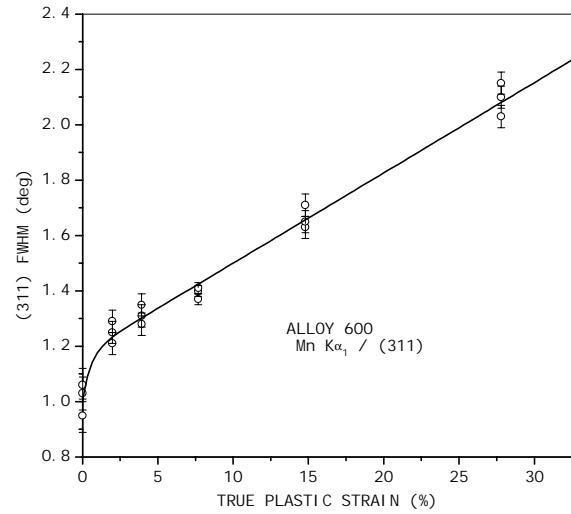


Fig. 2 Empirical relationship between (311) peak width and cold work (true plastic strain) for Alloy 600

Measurements were initially made on the machined inside surface of the sleeves prior to welding using copper $K\alpha$ radiation and the (420) planes, and after welding using manganese $K\alpha$ radiation and the (311) planes. The dependence of the (420) $K\alpha_1$ peak width on known amounts of cold work (true plastic strain) was previously developed empirically using specimens of Alloy 600 steam generator tubing which were first fully annealed and then pulled in tension to known levels of true plastic strain.⁽¹²⁾ During this investigation the same Alloy 600 samples were used to establish the dependence of the manganese $K\alpha$ (311) diffraction peak on true plastic strain shown in Fig. 2.

The yield strength increase associated with the amount of cold working at each measurement location and depth was, in turn, estimated using a true stress-strain curve from the equivalent true plastic strain. The true stress-strain curve for the Alloy 600 material involved

in the field failures is presented in Fig. 3 to nominally 27% strain. The bulk yield strength is nominally 434 MPa, and approximately doubles when the alloy is cold worked 25%, as seen in Fig. 3. As will be shown in the results obtained, the amount of cold work induced in machining Alloy 600 can readily exceed the nominally 27% cold work achieved in tension to produce the data shown in Fig. 3. It was therefore necessary to extrapolate to estimate yield strengths beyond the range of the true stress-strain curve. The ultimate tensile strength (UTS) will also increase with prior cold work. The published (engineering) UTS⁽¹³⁾ for annealed tubing is 772 MPa, well below the yield strength of material cold worked to 25%.

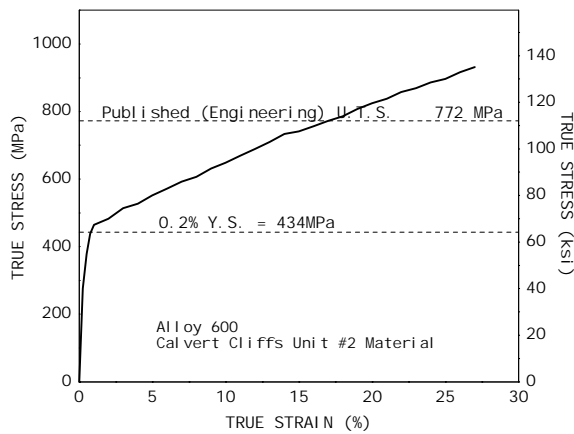


Fig. 3 - True stress-strain curve measured for Alloy 600 heater sleeve material removed from service.

RESULTS AND DISCUSSION

The circumferential and axial sectioning relaxation results obtained at the low side of the Alloy 600 heater sleeve J-weld mockup are presented in Fig. 4, as functions of distance from the top of the weld overlay. Relaxations were found to be relatively high, ranging to -500 MPa for the circumferential direction HAZ. The axial relaxation became tensile at distances greater than approximately 7 mm into the constraining steel block. The relaxations shown here are substantially higher than those observed on the high angle side,⁽³⁾ presumably due to the greater constraint provided by the carbon steel block on the high side. The sectioning relaxation was subtracted algebraically from the XRD

results, assuming elastic superposition, to determine the total residual stress when the J-weld mockup was whole. The relaxation was assumed to be constant from the inside surface to the maximum depth of 0.25 mm examined.

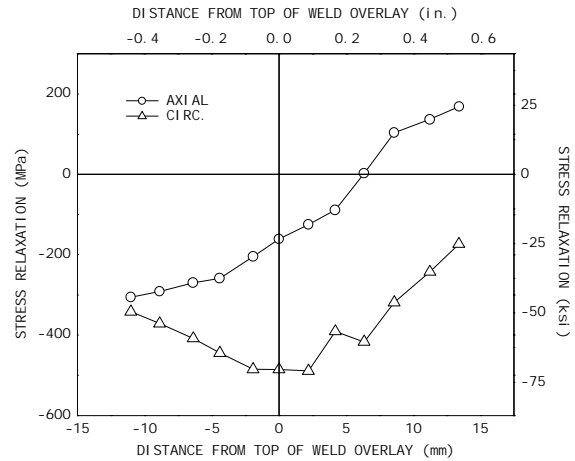


Fig. 4 - Axial and circumferential residual stress relaxations monitored on the inside surface of the Alloy 600 sleeve after longitudinal sectioning.

The residual stress and cold work distributions produced by reaming the inside diameter surface of the Alloy 600 sleeves were measured on a separate portion of a sleeve which was not welded. The residual stress and (420) peak width distributions obtained as functions of depth in the drawn and reamed areas are shown in Fig. 5. The results are plotted using the same residual stress scale later employed for the welded specimen.

The stress distributions remaining after the initial tubing fabrication, are compressive in both the circumferential and axial directions, less than -200 MPa, from the surface to a depth of nominally 125 μ m.

After reaming, the axial direction is more compressive to the maximum depth examined, and the circumferential direction was found to be nearly stress free. The (420) peak width distributions shown at the bottom of Fig. 5 reveal that the reaming operation induces more cold work, to a deeper depth, than the initial drawing. The amount of cold work, estimated from the empirical curve shown in Fig. 2, is nearly 25% at the inside surface of the drawn tube, and over 50% after reaming, as shown in Fig 6.

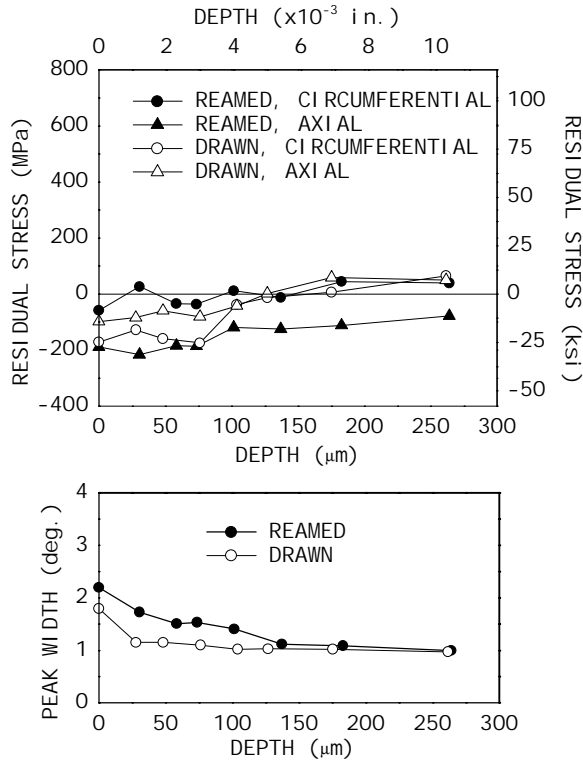


Fig. 5 - Baseline subsurface axial and circumferential residual stress and (420) peak width distributions for drawn and reamed Inconel 600 sleeve removed from service.

Deformation from reaming extends to 150 μm beneath the surface. The corresponding yield strength, estimated from the true stress-strain curve in Fig. 3, is on the order of 900 to 1000 MPa at the deformed surface of the reamed areas. The yield strength drops rapidly to near the nominal bulk value of 443 MPa at a depth of only 25 μm for the drawn surface, but remains well above the nominal yield to a depth of approximately 150 μm , for the reamed surface, diminishing nearly linearly with depth.

The (311) peak width distributions measured as a function of axial displacement and depth on the Alloy 600 J-weld mockup are presented in Fig. 7. The area which was reamed, shown from nominally -40 to -16 mm at the left side of the figure, is the most highly deformed, with a maximum evident at all depths at the edge of the reamed area nearest to the HAZ. The HAZ, shown as the inside surface opposite the actual weld fusion zone, ranges from approximately -8 to +18 mm. The material from +18 to +26 mm, at the right of Fig. 7, was deformed only during the original tubing fabrication prior to welding.

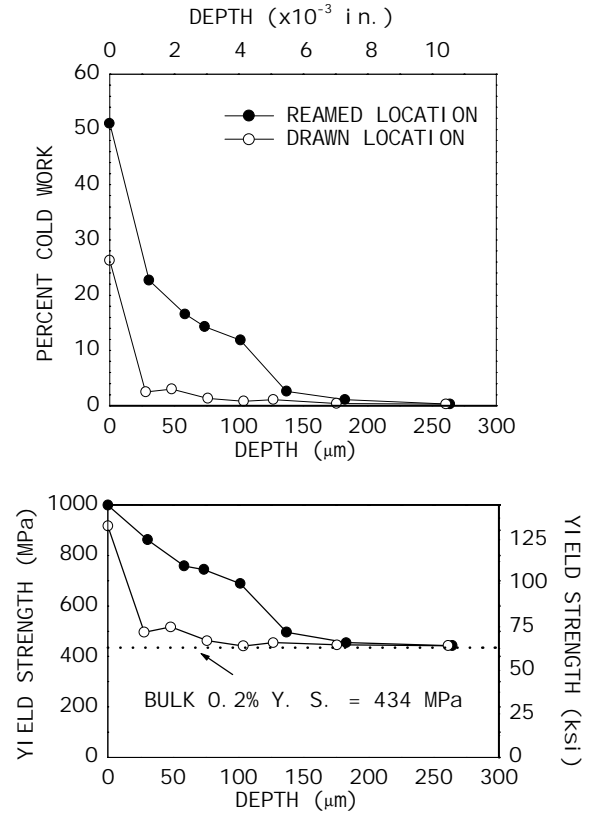


Fig. 6 Subsurface percent cold work (equivalent accumulated true plastic strain) and corresponding yield strength distribution for baseline drawn and reamed locations on Alloy 600 sleeves removed from service.

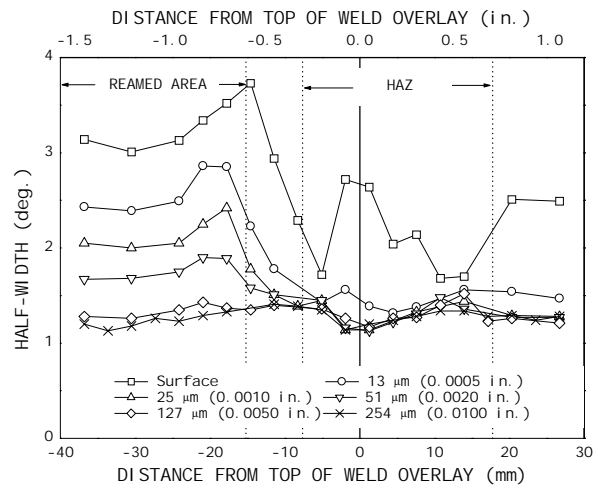


Fig. 7 Variation in (311) peak width with axial displacement and depth through the HAZ and machined regions on the low side of the 50° Alloy 600 J-weld mockup

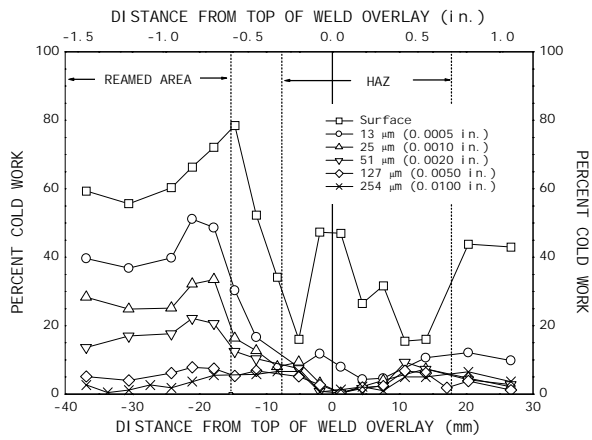


Fig. 8 Variation in degree of cold work (equivalent accumulated true plastic strain) with axial displacement and depth in the HAZ and machined regions of the low-angle side of the 50° Alloy 600 J-weld mockup

The estimated cold work distributions are presented in Fig. 8. The reamed surface layers are the most deformed, with the reamed surface, remote from the weld, deformed nearly 60% at -37 mm, comparable to the results obtained on the reamed surface prior to welding shown in Fig. 6. An increase in the amount of cold work in the reamed area, attributed to additional cold working caused by weld shrinkage at the edge of the HAZ, is evident at virtually all depths between approximately -20 and -15 mm. At a depth of 254 μm, the material is free of cold work in the reamed zone beyond approximately -30 mm and in the original drawn tubing beyond approximately 25 mm. All layers deeper than nominally 25 μm appear to be fully annealed in the center of the HAZ. Weld shrinkage has deformed the Alloy 600 nominally 5% from approximately 5 to 25 mm on either side of the fusion line. The inside surface still retains in excess of 40% cold work at the center of the HAZ, indicating only depths greater than 25 μm were fully annealed during welding to the outside surface of the sleeve.

The yield strength distributions, estimated from the true stress-strain curve, are presented in Fig. 9. Because the degree of cold work produced by machining exceeded the range of the true stress-strain curve, yield strengths in excess of nominally 900 MPa have been extrapolated. The yield strength in the reamed area outside the HAZ exceeds the nominal bulk engineering yield stress of 443 MPa at all depths from the surface down to 127 μm. After

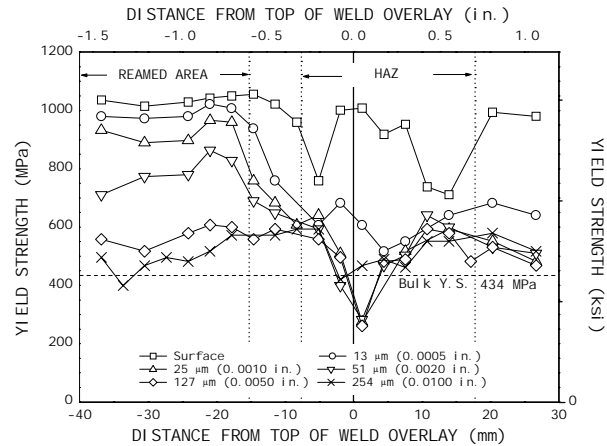


Fig. 9 Variation in yield strength with axial displacement and depth in the HAZ and machined regions of the low-angle side of the 50° Alloy 600 J-weld mockup, relative to the bulk yield strength

the severe deformation produced by reaming, the surface and 13 μm depths in the HAZ are capable of supporting residual stresses well in excess of the published engineering yield strength of the material, because these depths were not fully annealed during welding. The yield strength at the surface of the drawn region, beyond 20 mm, is significantly increased from the surface to a depth of 13 μm.

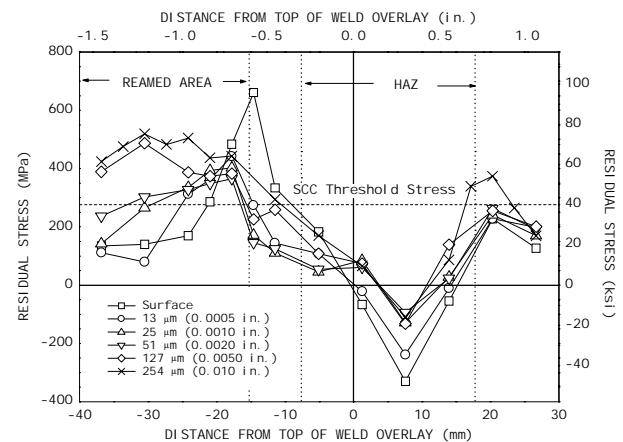


Fig. 10 Variation in axial residual stress with axial displacement and depth through the HAZ and machined regions on the low-angle side of the 50° J-weld Alloy 600 mockup.

The axial and circumferential macroscopic residual stress distributions are presented as functions of axial position and depth in Fig. 10 and 11. As a

consequence of the complex thermal-mechanical history of the weld fusion region, the residual stress distributions are also quite complex. The most tensile residual stresses were produced in the reamed area adjacent to the HAZ. This region is close enough to the fusion zone for significant weld shrinkage to pull the cold worked surface into tension, but too far for significant annealing during welding. The axial stress rises into tension to +650 MPa at approximately -15 mm. The axial tension diminishes rapidly with depth, but exceeds the stress corrosion threshold in the reamed region between -17 mm and -25 mm at the edge of the reamed area nearest the HAZ at all depths examined. The increase in axial tension with increasing depth in the reamed region between -30 mm and -40 mm, is attributed to distortion of the sleeve caused by weld shrinkage. The axial residual stresses in the HAZ are seen to be beneath the stress corrosion threshold, and even entirely compressive, at all depths examined approximately 8 mm into the block. The axial stresses return to tension, nearly uniform with depth, in the unreamed area beyond nominally 18 mm.

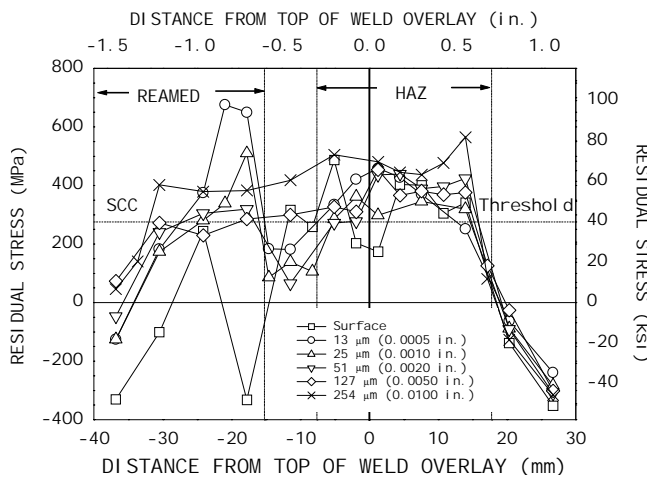


Fig 11 Variation in circumferential residual stress with axial displacement and depth on the low-angle side of the 50° Alloy 600 J-weld mockup showing stresses greater than the SCC threshold.

The circumferential residual stress distributions, shown in Fig. 11, are tensile, generally in excess of the stress corrosion cracking threshold, and highest just beneath the surface at 13 μm in the reamed area adjacent to the HAZ. The Alloy 600 is in tension from -30 mm to +18 mm, and most uniformly in tension at the maximum depth of 250 μm examined. The circumferential stress is on the order of the bulk yield strength of the material at the 254 μm depth between -30 mm and +12 mm, attributed to radial yielding of the undeformed material

below the layer deformed by reaming. The nearly uniform tension is attributed to weld shrinkage expanding the sleeve radially in the steel block. The stress distributions are entirely compressive in the circumferential direction at all depths in the unreamed material beyond 20 mm into the block.

CONCLUSIONS

The high resolution x-ray diffraction study of the residual stress, cold work, and yield strength distributions in the Alloy 600 J-weld penetration provide an excellent example of the use of XRD to characterize the complex residual stress and mechanical property distributions produced in actual machined and welded components. Several conclusions appear to be supported by the results obtained:

- The cold work produced by the combination of machining and weld shrinkage alters the mechanical properties, specifically the yield strength, of the deformed surface layers. The yield strength of the deformed material is well in excess of the bulk yield for the alloy, and is therefore capable of supporting residual stresses correspondingly higher.
- The residual stress and yield strength distributions can vary rapidly with depth and position, producing very localized areas susceptible to SCC.
- Alloy 600 may be cold worked over 50% by machining processes such as reaming and at least an additional 5% by weld shrinkage in a constrained geometry, resulting in yield strengths greater than 900 MPa on the reamed surface and 600 MPa adjacent to the HAZ in material not previously deformed by machining.
- The cold work due to weld shrinkage is accumulative, being additive to the prior cold work produced by machining, as seen in the reamed area adjacent to the HAZ.
- The residual stresses developed by welding depend upon the yield strength and residual stress distributions produced by prior machining.
- The residual stress and yield strength distributions produced by prior machining should be considered in the development of any finite element predictive

model of welding residual stresses.

- Control of the cold working of the surface during machining may offer an opportunity to minimize the residual stresses developed during subsequent weld fabrication of nuclear components.

ACKNOWLEDGEMENTS

The authors acknowledge the assistance of ABB Combustion Engineering for preparing the samples, providing the true stress-strain data and many helpful discussions, and Dr. R. S. Pathania of EPRI for support for the sample fabrication and the initial investigation of J-weld residual stresses under EPRI contract no. RP3223-02.

REFERENCES

1. J.F. Hall and D.B. Scott, Destructive Examination of Pressurizer Heater Sleeves from Calvert Cliffs Unit 2, *Report CE-NPSD-577*, October 1989.
2. J.A. Gorman, "Status and Suggested Course of Action for Nondenting-Related Primary-Side IGSCD of Westinghouse-Type Steam Generators," *EPRI, Report MP-4594-LD*, May 1986.
3. J.F. Hall, J.P. Molkenhuth, and P.S. Prevéy, XRD Residual Stress Measurements on Alloy 600 Pressurizer Heater Sleeve Mockups, *Proceedings of the Sixth International Symposium on Environmental Degradation of Materials in Nuclear Power Systems-Water Reactors*, (San Diego, CA: TMS, ANS, NACE, 1993), pp 855-861.
4. J.F. Hall, J.P. Molkenhuth, P.S. Prevéy, and R.S. Pathania, Measurement of Residual Stresses in Alloy 600 Pressurizer Penetrations, *Conference on the Contribution of Materials Investigation to the Resolution of Problems Encountered in Pressurized Water Reactors*, (Paris: Societe Francaise d'Energie Nucleaire, Sept. 12-16, 1994).
5. *Alloy Digest*, Inconel Alloy 600 Spec. Sheet Ni-176, (Upper Montclair, NJ: Eng. Alloys Dig., July, 1972).
6. *Woldman's Engineering Alloys*, 6th Edition, R.C. Gibbons, Ed., American Society for Metals, 1979, p. 747.
7. M.E. Hilley, ed., *Residual Stress Measurement by X-Ray Diffraction, SAE J784a*, (Warrendale, PA: Society of Auto. Eng., 1971).
8. I.C. Noyan and J.B. Cohen, *Residual Stress Measurement by Diffraction and Interpretation*, (New York, NY: Springer-Verlag, 1987).
9. B.D. Cullity, *Elements of X-ray Diffraction*, 2nd ed., (Reading, MA: Addison-Wesley, 1978), pp. 447-476.
10. P.S. Prevéy, "X-Ray Diffraction Residual Stress Techniques," *Metals Handbook*, Vol 10, (Metals Park, OH: ASM, 1986), pp 380-392.
11. P.S. Prevéy, "A Method of Determining Elastic Properties of Alloys in Selected Crystallographic Directions for X-Ray Diffraction Residual Stress Measurement," *Adv. In X-Ray Analysis*, Vol. 20, (New York, NY: Plenum Press, 1977), pp 345-354.
12. P.S. Prevéy, "The Use of Pearson VII Functions in X-Ray Diffraction Residual Stress Measurement," *Adv. in X-Ray Analysis*, Vol. 29, (New York, NY: Plenum Press, 1986), pp 103-112.
13. P.S. Prevey, "The Measurement of Residual Stress and Cold Work Distributions in Nickel Base Alloys," *Residual Stress in Design, Process and Material Selection*, (Metals Park, OH: ASM, 1987).
14. P.S. Prevéy, "Surface Residual Stress Distributions in As-Bent Inconel 600 U-Bend and Incoloy 800 90-Degree Bend Tubing Samples," *Workshop Proceedings: U-Bend Tube Cracking in Steam Generators*, (Palo Alto, CA: EPRI, 1981), pp 12-3 to 12-9.